Chemical Engineering Science 303 (2025) 120926

Contents lists available at ScienceDirect

Chemical Engineering Science

journal homepage: www.elsevier.com/locate/ces

On a new globally optimal method for the design optimization of air coolers coupled with real fans

Marco Thiago da C. Santos [a], Argimiro Resende Secchi [c], Miguel J. Bagajewicz [b,d], André L.H. Costa [a,*]

[a] Institute of Chemistry, Rio de Janeiro State University (UERJ), Rio de Janeiro, Brazil
[b] School of Chemistry, Federal University of Rio de Janeiro (UFRJ), Rio de Janeiro, Brazil
[c] Chemical Engineering Program, COPPE, Federal University of Rio de Janeiro (UFRJ), Rio de Janeiro, Brazil
[d] School of Sustainable, Chemical, Biological, and Materials Engineering, University of Oklahoma, OK, USA

ARTICLE INFO

Keywords:
Air cooler
Design
Optimization
Set Trimming
Smart Enumeration

ABSTRACT

A new approach for the globally optimal design of air coolers is presented. First, by coupling the air cooler geometric options with commercially available fans, the traditional mismatch emerging from designing the air cooler first and selecting a commercial fan later is removed. Second, the method departs from the traditional LMTD and ε-NTU methods, adopting a model composed of a differential–algebraic system of equations (DAE system) for the air cooler simulation, which is discretized to consider properties variable with temperature. The resultant optimization problem is solved using Set Trimming and Smart Enumeration, which can identify the global optimum through the simulation of only a small fraction of the search space. The comparison of the simulation results with different commercial software provided similar outputs. A comparison with design results obtained using LMTD solutions indicates that the LMTD models may overdesign/underdesign the unit.

1. Introduction

Air is widely employed for cooling services due to several reasons: it is freely available, it presents less corrosion and fouling problems when compared to cooling water, it can be used without any special treatment, etc. (Paikert, 2008). In chemical and petroleum industries, the usual type of air-cooled heat exchangers involves a hot stream that flows throughout a set of horizontal finned tubes and is cooled and/or condensed by ambient air moved by a fan or a set of fans. The finned surface is formed by annular fins arranged in a helical pattern (Serth, 2007). Tube bundles are employed in modular structures that can be mounted in banks composed of a set of parallel bays, a bay is a structure formed by one or more tube bundles served by the same set of fans (Saunders, 1988). Usually, this kind of heat exchanger is called an air cooler, aerial cooler, or fin fan cooler. Thus, the term air cooler is used throughout the rest of this paper to designate this kind of air-cooled heat exchanger. Air coolers are the second most used type of heat exchanger in chemical and petroleum processing industries (Serth, 2007). Unlike shell-and-tube heat exchangers, which make use of cooling water, they are particularly useful when there is water scarcity, like in arid regions or highly dense industrial areas (Saunders, 1988).

Traditionally, the literature on the design of heat exchangers recommends using trial-and-verification procedures, where successive candidate solutions are proposed until one fulfills the thermal and fluid dynamic constraints. The procedure does not usually intend to optimize the design; rather just a viable design suffices most of the time (Costa and Bagajewicz, 2019).

The use of optimization techniques brings important cost reductions in engineering systems. Previous attempts in the design optimization of air coolers involved mainly metaheuristics or mathematical programming.

Metaheuristic techniques are based on algorithms involving randomized steps. Doodman et al. (2009) applied a harmony search algorithm to obtain the optimal design of air coolers. Before the optimization, the authors employed a global sensitivity analysis to select the optimization variables. The results revealed that the proposed algorithm was superior to genetic algorithms for this kind of problem. An Imperialist Competitive algorithm was implemented by Karami et al. (2012) and Rezaei et al. (2012) to optimize the heat transfer in air coolers using twisted tape inserts and butterfly inserts, respectively. A new multi-objective optimization approach using a genetic algorithm

* Corresponding author.
E-mail address: andrehc@uerj.br (A.L.H. Costa).

https://doi.org/10.1016/j.ces.2024.120926
Received 19 August 2024; Received in revised form 3 November 2024; Accepted 9 November 2024
Available online 12 November 2024

Nomenclature

Ab	Exposed area of the root tube, m^2
$Aface$	Air Cooler face area, m^2
Aof	Fin area, m^2
Aot	Total finned surface area per unit length, m^2/m
Ar	Outer tube bare area per unit length, m^2/m
Cpc	Air heat capacity, J/(kg·K)
Cph	Hot stream heat capacity, J/(kg·K)
Df	Fin diameter, m
$Dfan$	Fan diameter, m
Dte	Tube outer diameter, m
Dti	Tube inner diameter, m
FAR	Free Area Ratio
fc	Airstream friction factor, dimensionless
fh	Tube-side stream friction factor, dimensionless
Gc	Airstream mass flux, kg/m^2
Gh	Hot stream mass flux, kg/m^2
Gn	Hot stream mass flux in the nozzle, kg/m^2
h'	Corrected airstream heat transfer coefficient, W/m^2 K
hc	Airstream heat transfer coefficient, $W/(m^2 \cdot K)$
hh	Hot stream heat transfer coefficient, $W/(m^2 \cdot K)$
J	Number of discretized points
kc	Air thermal conductivity, W/(m·K)
kf	Fin thermal conductivity, W/(m·K)
kh	Hot stream thermal conductivity, W/(m·K)
kt	Tube wall thermal conductivity, W/(m·K)
L	Tube length, m
Lf	Fin height, m
Lfe	Corrected fin length, m
Ltp	Tube pitch, m
$\widehat{m}c$	Airstream mass flow rate, kg/s
$\widehat{m}h$	Hot stream mass flow rate, kg/s
$Nbay$	Number of bays
$Nbbay$	Number of bundles per bay
Nf	Number of fins per unit length, m^{-1}
$Nfanbay$	Number of fans per bay
Np	Number of tube passes
Nr	Number of rows
Ntr	Number of tubes per row
Ntt	Total number of tubes
Nuc	Airstream Nusselt number, dimensionless
Nuh	Tube side stream Nusselt number, dimensionless
Prc	Airstream Prandtl number, dimensionless
Prh	Tube side stream Prandtl number, dimensionless
R	Number of tube rows per pass
$Reeff$	Airstream Reynolds number considering fins, dimensionless
Rec	Airstream Reynolds number, dimensionless
Reh	Tube side stream Reynolds number, dimensionless
$\overline{Rehn}$	Tube side stream Reynolds number on the nozzles, dimensionless
$\widehat{Rfc}$	Airstream fouling factor, m^2K/W
$\widehat{Rfh}$	Tube side stream fouling factor, m^2K/W
sf	Fin spacing, m
$qbundle$	Air volumetric flow rate per bundle, m^3/s
$qfan$	Air volumetric flow rate per fan, m^3/s
Tc	Air temperature, °C
$\overline{T}c$	Average air temperature between two consecutive rows, °C
$\widehat{Tci}$	Air inlet temperature, °C
Tco	Air outlet temperature, °C
tf	Fin thickness. m
Th	Hot stream temperature, °C
$\overline{T}h$	Average hot stream temperature for midpoint method, °C
$\widehat{Thi}$	Hot stream inlet temperature, °C
Tho	Hot stream outlet temperature, °C
Thx	Hot stream temperature inside the header, °C
U	Overall heat transfer coefficient, $W/(m^2 \cdot K)$
vc	Airside velocity, m/s
W	Bundle width, m
$Wused$	Power consumption per fan, W
x, y, z	Cartesian coordinates
ΔPc	Airside pressure drop across the air cooler, Pa
$\Delta Pfan$	Total air side pressure drop, Pa
ΔPh	Total tube side pressure drop, Pa
ΔPhf	Pressure drop by pipe friction per row, Pa
$\Delta Phfr$	Pressure drop by pipe friction per pass, Pa
$\Delta Phft$	Total pressure drop by pipe friction, Pa
ΔPn	Pressure drop on the nozzles, Pa
$\Delta Phrin$	Pressure drop in the entrance header, Pa
$\Delta Phrout$	Pressure drop in the exit header, Pa
$\Delta Phrx$	Pressure drop in the return headers, Pa
μc	Air viscosity, Pa·s
μh	Hot stream viscosity, Pa·s
ηf	Fin efficiency
ηfan	Fan efficiency
$\eta motor$	Motor efficiency
ηsr	Space reductor efficiency
ηt	Overall efficiency of the finned surface
ρc	Air density, kg/m^3
ρh	Hot stream density, kg/m^3
γ	Interpolation factor

Subscripts

b	bundle
$exit$	At the end of the tube
j	Finite Volume discretization
out	Leaving the unit by the air side
p	Tube Pass
r	Row
tot	Total

was proposed by Kashani et al. (2013), the conflicting objective functions were the temperature approach and the total annual cost. Based on an additional selection procedure, a final optimum point is attained.

Mathematical programming techniques involve the solution of the optimization problem using deterministic algorithms based on optimality conditions and/or differential approximations. González et al. (2001) used nonlinear programming (NLP) based on a sequential quadratic programming algorithm (SQP) to solve the air cooler design problem. Manassaldi et al. (2014) solved the design problem using a mixed-integer nonlinear programming (MINLP) algorithm. Souza et al. (2018) presented a rigorous linear formulation of the model that was solved using a mixed-integer linear programming (MILP) procedure.

A different approach was explored by Carvalho et al. (2019), which pointed out that the airflow rate is a direct consequence of the hydraulic interaction between the tube bundles and the fan, and a mechanical energy balance is needed, involving the system curve and the fan curve. Thus, Carvalho et al. (2019) addressed the design problem using an LMTD-based model associated with a fluid dynamic model of the airflow considering the fan performance. These authors obtained the global optimum of the design problem using Set Trimming followed by Smart Enumeration (Costa and Bagajewicz, 2019).

Despite the use of different optimization techniques, all of these

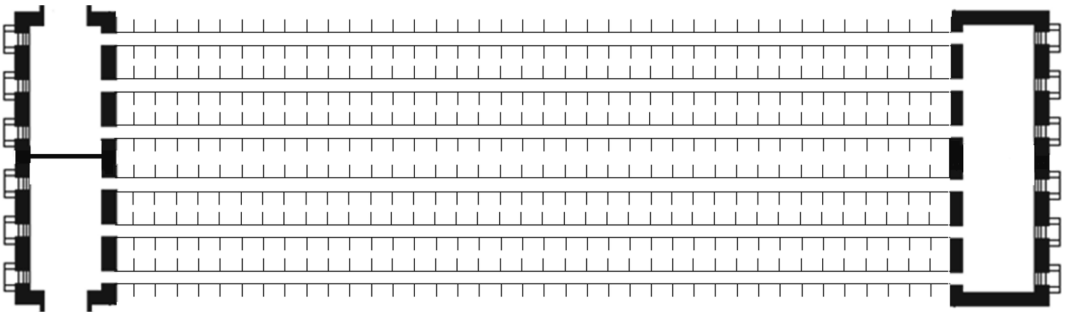

Fig. 1. Tube bundle composed of 2 passes with 3 tube rows per pass.

papers have one point in common: the utilization of air cooler models based on analytical solutions, e.g. the LMTD or the ε-NTU methods. These methods are based on the assumption of uniform physical properties and heat transfer coefficients along the heat transfer surface. Despite its simplicity and wide utilization, these methods present accuracy limitations when the physical properties vary significantly with the temperature. This aspect of previous work hinders the utilization of these optimization approaches for real problems.

Because of the limitations of the analytical solutions, the literature presents several papers that addressed the modeling and simulation of air-cooled heat exchangers using numerical solutions based on the discretization of the problem domain, particularly focusing on refrigeration applications (Jiang et al., 2006; Sarfraz et al., 2019; Garcia et al., 2022). However, the complexity of these models and their ad-hoc formulation for each system to be simulated hinders its utilization for design optimization problems. There are papers in the literature that employed discretized models for the optimization of specific air-cooled heat exchangers applied to refrigeration systems (Ploskas et al., 2018; Li et al., 2019), but, as far as the authors could find, methods using discretized models to get optimal designs of air coolers employed for cooling process streams in chemical and petroleum industries do not exist. Software packages like HTRI and Aspen EDR employ air cooler models based on proprietary equations and consider the changes in properties as a function of temperature. They describe little about the equations they use and their numerical integration procedures, other than saying that they use "zones", which are, presumably, discrete elements. These tools are available for purchase, but there is no free alternative to solve the rating and simulation problems in the open literature for the air coolers employed in the chemical and petroleum industries. In addition, the design results obtained are neither locally, nor globally optimal.

Aiming at circumventing these drawbacks, the current paper presents an air cooler design optimization approach using a discretized model of the energy and flow differential equations. The resultant mathematical model corresponds to a differential–algebraic system of equations (DAE system). The proposed model can represent the variation of the physical properties and the heat transfer coefficients along the heat transfer area. The optimal design problem is solved using Partial Set Trimming and Smart Enumeration (Costa and Bagajewicz, 2019). Different from previous optimization approaches, which can be trapped in a local optimum (except for Souza et al., 2018), this approach always identifies the global optimum.

The air cooler model employed by the design optimization is also novel, because it is based on a full parameterization of the air cooler configuration, i.e. any investigated air cooler structure can be simulated through only a proper selection of a given set of parameters. Therefore, the proposed model can be useful for further optimization works, because it provides a search space of design variables directly linked to a rigorous model. The results presented here indicate that the proposed model has an accuracy similar to commercial software programs.

Another aspect of the proposed model is the inclusion of the fan model in the mechanical energy balance. As a consequence, the airflow rate is evaluated according to the current fan curve. This feature of the model provides a more realistic representation of the optimal design problem because the air flow rate is not considered an independent optimization variable as in previous models, the actual design variable related to the airflow is the fan selection.

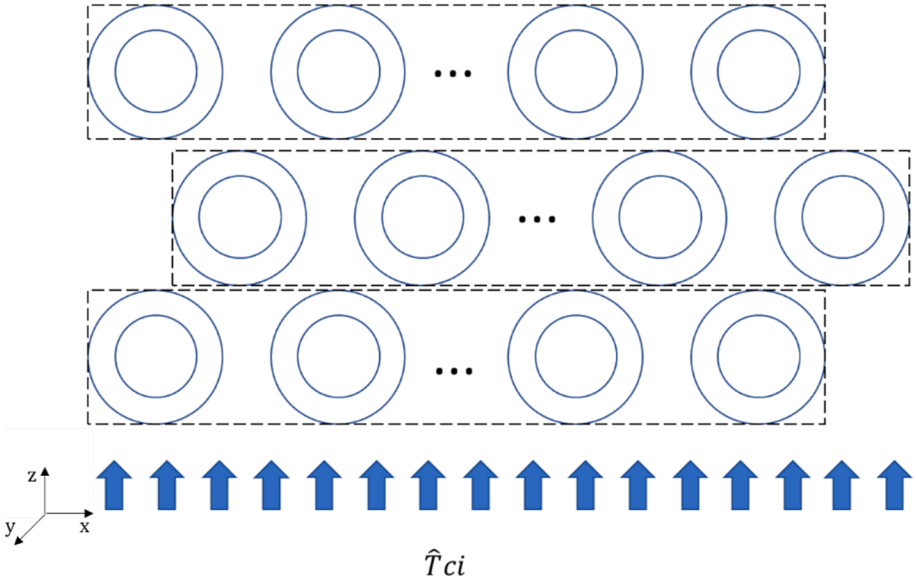

Fig. 2. Air cooler geometry.

The rest of this paper is organized as follows. Section 2 presents the representation scheme employed to describe the air cooler structure for any number of bays, bundles, and tube rows. Sections 3 and 4 present the thermal and fluid dynamic models, respectively, including the numerical discretization procedure. The simulation procedure to solve both models is presented in Section 5. Section 6 presents the optimization problem and the technique employed to identify the air cooler alternative with the lowest total annualized cost. Section 7 depicts the results of the performance of the model and the optimization procedure. Finally, Section 8 presents the conclusions.

2. Air cooler representation

The proposed model addresses air coolers composed of *Nbay* bays. Each bay contains *Nfanbay* fans and is formed by *Nbbay* tube bundles. Each tube bundle has *Np* passes and each pass contains *R* tube rows, therefore each tube bundle has $Nr = Np \times R$ rows of tubes. The tube rows are formed by *Ntr* parallel tubes uniformly distributed along the tube bundle width, therefore the total number of tubes in a tube bundle is: $Ntt = Nr \times Ntr$.

The identification of each row in the tube bundle employs two indices: $p = 1,\cdots,Np$, which identifies the tube passes, and $r = 1,\cdots,R$, which identifies the rows in a certain pass (both indices counting from top to bottom). Fig. 1 shows a tube bundle composed of two passes and three rows per pass (i.e. $p \in \{1,2\}$, $r \in \{1,2,3\}$, $Np = 2$, $R = 3$, and $Nr = 6$).

Fig. 2 shows a front view of a set of tube rows. The temperature of the hot stream inside the tubes, $Th_{p,r}$, varies along the length of the tubes (y axis). The air flows perpendicularly to the tubes (z axis), therefore its temperature varies along the different tube rows. The description of the temperature field associated with the airflow outside the tube rows is based on the values of the air temperatures between consecutive tube rows, where $Tc_{p,r}$ is the air temperature above the tube row *r* of the pass *p*.

3. Thermal model

The main governing equations for the steady-state thermal simulation of air coolers are energy balances, applied to the hot stream that flows inside the tubes and the air stream that flows outside the tubes. Additionally, energy balances in the tube bundle headers are also present in the model. The physical properties depend on the temperature, resulting in heat transfer coefficients varying along the exchanger. The variation of the physical properties with pressure is not considered in the model. It is assumed that the airflow is uniformly distributed throughout the tube bundle. In the model presentation below, the parameters are indicated with a symbol ˆ on top.

3.1. Energy balances

The thermal model of the tube-side flow corresponds to a unidimensional energy balance applied to an entire tube row *r* of a pass *p* in each tube bundle. Neglecting the diffusion term along the flow direction and assuming a stream without phase change, the corresponding differential equation is:

$$\frac{dTh_{p,r}}{dy} = (-1)^p \frac{U_{p,r}\, Aot\, Ntr \left(Th_{p,r} - Tc_{p,r}^{avg}\right)}{\widehat{mh}_b Cph_{p,r}},\ \forall p;\ \forall r \tag{1}$$

where $U_{p,r}$ is the overall heat transfer coefficient, *Aot* is the total finned surface area per unit length, $\widehat{mh}_b$ is the mass flowrate of the hot stream per bundle, $Cph_{p,r}$ is the heat capacity of the hot stream. The driving force of the heat transfer in Eq. (1) is represented by the difference between the hot stream temperature and the average of the air temperatures above and below the tube row:

$$Tc_{p,r}^{avg} = \frac{Tc_{p,r} + Tc_{p,r-1}}{2},\ 1 < p \le Np;\ 1 < r \le R \tag{2}$$

$$Tc_{p,r}^{avg} = \frac{Tc_{p,r} + Tc_{p-1,R}}{2},\ 1 < p \le Np;\ r = 1 \tag{3}$$

$$Tc_{p,r}^{avg} = \frac{Tc_{p,r} + Tco}{2},\ p = 1;\ r = 1 \tag{4}$$

where *Tco* is the air outlet temperature from the heat exchanger.

The energy balance for the airflow around a tube row is given by:

$$U_{p,r}\, Aot\, Ntr\left(Th_{p,r} - Tc_{p,r}^{avg}\right) - \frac{mc_b}{L}\left(\frac{Cpc_{p,r} + Cpc_{p,r-1}}{2}\right)\left(Tc_{p,r-1} - Tc_{p,r}\right) = 0,\ \forall p;\ 1 < r \le R \tag{5}$$

$$U_{p,r}\, Aot\, Ntr\left(Th_{p,r} - Tc_{p,r}^{avg}\right) - \frac{mc_b}{L}\left(\frac{Cpc_{p,r} + Cpc_{p-1,R}}{2}\right)\left(Tc_{p-1,R} - Tc_{p,r}\right) = 0,\ 1 < p \le Np;\ r = 1 \tag{6}$$

$$U_{p,r}\, Aot\, Ntr\left(Th_{p,r} - Tc_{p,r}^{avg}\right) - \frac{mc_b}{L}\left(\frac{Cpc_o + Cpc_{p,r}}{2}\right)\left(Tc_o - Tc_{p,r}\right) = 0,\ p = 1;\ r = 1 \tag{7}$$

where *L* is the tube length, mc_b is the air mass flow rate per tube bundle and $Cpc_{p,r}$ is the heat capacity of the air.

At the end of a pass, there is a header where the hot stream from each tube row of the same pass is mixed. Therefore, the corresponding energy balance is simplified to consider locally constant heat capacity:

$$\frac{\sum_{r=1}^{R} Cph_{p,r,exit} Th_{p,r,exit}}{R} = Cpx_p Thx_p,\ \forall p \tag{8}$$

where $Th_{p,r,exit}$ is the hot stream temperature at the tube outlet, Thx_p is the temperature at the downstream header of the pass *p*, and $Cph_{p,r,exit}$ and Cpx_p are the corresponding heat capacities of the hot stream.

The above set of equations together with the equations for the calculation of the heat transfer coefficient form a DAE system, which is later discretized in the tube flow direction (axis *y*).

The relations between the mass flow rates of the hot and air streams in each bundle and the corresponding values of the total mass flow rates, $\widehat{mh}_{tot}$ and mc_{tot}, are given by:

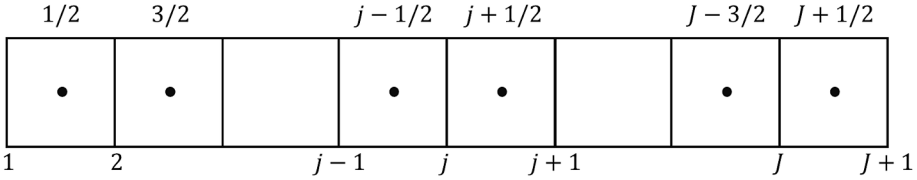

Fig. 3. Finite volumes of a grid with *J* elements and index notation for cell centers and cell faces.

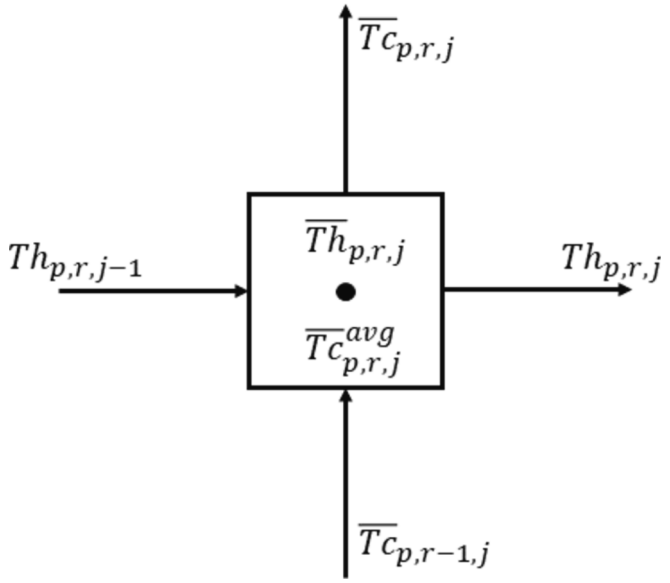

Fig. 4. Finite-volume element.

$$\widehat{mh}_b = \frac{\widehat{mh}_{tot}}{Nbay\ Nbbay} \tag{9}$$

$$mc_b = \frac{mc_{tot}}{Nbay\ Nbbay} \tag{10}$$

3.2. Discretization

The finite-volume method was employed to discretize the governing DAE system. A staggered grid is chosen to describe the problem. The grid divides the air cooler tubes into multiple cells along the direction of the flow path of the hot stream. The governing equations are integrated into the volume of each cell, leading to algebraic equations, where the temperatures are evaluated in the cell faces. With this grid, the average temperature is located at the center of the element, as summarized in Figs. 3 and 4.

3.2.1. Interpolation scheme

The central differencing scheme (CDS) can cause numerical oscillations. Despite its higher stability, the first-order upwind scheme may require a large number of elements to obtain an accurate solution. Thus, the midpoint method, which can guarantee both stability and second-order accuracy (Archer and Petzold, 1998) is used. Thus, temperatures are evaluated at the cell face and the equation is evaluated at the center of the cell.

3.2.2. Discretized energy balances

Entering each pass, the hot stream is divided among the rows. When leaving each pass, all the streams coming from the rows are mixed in the header. The direction of the flow changes from one pass to the next one in each pass changes: odd passes have the direction from left to right (from $j = 1$ to $j = J + 1$) and even passes have the opposite direction (from $j = J+1$ to $j = 1$).

The differential equations of the energy balance represented in Eq. (1) and Eq. (7) become:

$$\left(Th_{p,r,j} - Th_{p,r,j-1}\right) = (-1)^p \frac{\overline{U}_{p,r,j} Aot\ R\ Ntr\ L\left(\overline{Th}_{p,r,j} - \overline{Tc}^{avg}_{p,r,j}\right)}{J\ \widehat{mh}_b Cph_{p,r,j}},\ \forall p;\ \forall r;\ 1 < j \le J+1 \tag{11}$$

According to the midpoint method, the average temperature of the hot and cold streams in Eq. (7) are given by:

$$Th_{p,r,j+1/2} = \overline{Th}_{p,r,j} = \frac{Th_{p,r,j} + Th_{p,r,j-1}}{2},\ \forall p;\ r = 1,\ldots,R;\ 1 < j \le J+1 \tag{12}$$

$$Tc^{avg}_{p,r,j+1/2} = \overline{Tc}^{avg}_{p,r,j} = \frac{\overline{Tc}^{avg}_{p,r,j} + \overline{Tc}^{avg}_{p,r,j-1}}{2},\ \forall p;\ 1 < r \le R;\ 1 < j \le J+1 \tag{13}$$

The overall heat transfer coefficient, $\overline{U}_{p,r,j}$, in Eq. (7) are calculated at the average temperatures expressed in Eq. (12) and Eq. (13).

The inlet hot stream temperature of each pass corresponds to the mixing temperature at the header from the previous pass, except for the first pass, where it corresponds to the hot stream inlet temperature in the heat exchanger:

$$Th_{p,r,j} = \widehat{Thi}\ ,\quad p = 1;\ r = 1,\ldots,R;\ j = 1 \tag{14}$$

$$Th_{p,r,j} = Thx_{p-1}\ ,\forall\ \text{odd}\ p \neq 1;\ r = 1,\ldots,R;\ j = 1 \tag{15}$$

$$Th_{p,r,j} = Thx_{p-1}\ ,\ \forall\ \text{even}\ p;\ r = 1,\ldots,R;\ j = J+1 \tag{16}$$

The mixing temperatures at the headers are given by:

$$\frac{\sum_{r=1}^{R} Cph_{p,r,J} Th_{p,r,J}}{R} = Cpx_p Thx_p,\ \forall\ \text{odd}\ p \tag{17}$$

$$\frac{\sum_{r=1}^{R} Cph_{p,r,1} Th_{p,r,1}}{R} = Cpx_p Thx_p,\ \ \forall\ \text{even}\ p \tag{18}$$

Finally, the airside energy balances are:

$$\begin{aligned} &U_{p,r,j}\ Aot\ Ntr\left(\overline{Th}_{p,r,j} - \overline{Tc}^{avg}_{p,r,j}\right) \\ &- \frac{mc_b}{L}\left(\frac{Cpc_{p,r,j} + Cpc_{p,r-1,j}}{2}\right)\left(\frac{\left(Tc_{p,r-1,j} + Tc_{p,r-1,j-1}\right)}{2}\right. \\ &\left. - \frac{\left(Tc_{p,r,j} + Tc_{p,r,j-1}\right)}{2}\right) \\ &= 0\ ,\ \ \forall p;\ 1 < r \le R;\ 1 < j \le J+1 \end{aligned} \tag{19}$$

$$\begin{aligned} &U_{p,r,j}\ Aot\ Ntr\left(\overline{Th}_{p,r,j} - \overline{Tc}_{p,r,j}\right) \\ &- \frac{mc_b}{L}\left(\frac{Cpc_{p,r,j} + Cpc_{p-1,R,j}}{2}\right)\left(\frac{\left(Tc_{p-1,R,j} + Tc_{p-1,R,j-1}\right)}{2}\right. \\ &\left. - \frac{\left(Tc_{p,r,j} + Tc_{p,r,j-1}\right)}{2}\right) \\ &= 0\ ,\ \ 1 < p \le Np;\ r = 1;\ 1 < j \le J+1 \end{aligned} \tag{20}$$

$$\begin{aligned} &U_{p,r,j}\ Aot\ Ntr\left(\overline{Th}_{p,r,j} - \overline{Tc}_{p,r,j}\right) - \frac{mc_b}{L}\left(\frac{Cpc_o + Cpc_{p,r,j}}{2}\right)\left(\frac{\left(Tc_{o,j} + Tc_{o,j-1}\right)}{2}\right. \\ &\left. - \frac{\left(Tc_{p,r,j} + Tc_{p,r,j-1}\right)}{2}\right) \\ &= 0 \qquad p = 1;\ r = 1;\ 1 < j \le J+1 \end{aligned} \tag{21}$$

Additionally:

$$Tc_{p,r,j} = \widehat{Tci}\ ,\quad p = Np;\ r = R;\forall j \tag{22}$$

3.3. Heat transfer coefficients

3.3.1. Hot stream

Depending on the Reynolds number, different equations are used for the determination of the local convective heat transfer coefficient of the hot stream on the tube side. For fully turbulent flow ($Reh \ge 10000$), the equation proposed by Seider and Tate (Serth, 2007), expanded to include entry effects (Gnielinksi, 2010) is used:

$$Nuh_{p,r,j} = 0.027 Reh_{p,r,j}^{0.8} Prh_{p,r,j}^{1/3} \left[1 + \frac{1}{3} \left(Dti \frac{J}{j\, L} \right)^{2/3} \right] \tag{23}$$

For laminar flow ($Reh \leq 2300$), the correlations suggested by Gnielinski (2010) for local Nusselt numbers, considering constant heat flux (the adoption of the correlations of constant heat flux for laminar flow provided results similar to the predictions of commercial software) are used:

$$Nuh1_{p,r,j} = 4.354 \tag{24}$$

$$Nuh2_{p,r,j} = 1.302 \sqrt[3]{Reh_{p,r,j} Prh_{p,r,j} \frac{Dti\, J}{j\, L}} \tag{25}$$

$$Nuh3_{p,r,j} = 0.462 \sqrt[3]{Prh_{p,r,j}} \sqrt{Reh_{p,r,j} \left(\frac{Dti\, J}{j\, L} \right)} \tag{26}$$

$$Nuh_{p,r,j} = \left\{ {Nuh1_{p,r,j}}^3 + \left(Nuh2_{p,r,j} - 1 \right)^3 + {Nuh3_{p,r,j}}^3 \right\}^{1/3} \tag{27}$$

Finally, Gnielinski (2010) proposed the evaluation of the Nusselt number for Reynolds numbers between 2300 and 10,000 (encompassing turbulent and transitional flow) through linear interpolation between the values of the Nusselt number calculated at the laminar condition for $Reh = 2300$ ($Nuh_{p,r,j,lam}^{2300}$) and the fully turbulent condition for $Reh = 10^4$ ($Nuh_{p,r,j,turb}^{10000}$):

$$Nuh_{p,r,j} = (1-\gamma) Nuh_{p,r,j,lam}^{2300} + \gamma Nuh_{p,r,j,turb}^{10000} \tag{28}$$

where γ is given by:

$$\gamma_{p,r,j} = \frac{Reh_{p,r,j} - 2300}{10^4 - 2300} \tag{29}$$

The expression of the Nusselt and Reynolds numbers in the correlations presented above are:

$$Nuh_{p,r,j} = \frac{hh_{p,r,j} Dti}{kh_{p,r,j}} \tag{30}$$

$$Reh_{p,r,j} = \frac{Dti\, Gh}{\mu h_{p,r,j}} \tag{31}$$

where $kh_{p,r,j}$ and $\mu h_{p,r,j}$ are the thermal conductivity and viscosity of the hot stream, $hh_{p,r,j}$ is the heat transfer coefficient of the hot stream, Dte is the outer tube diameter and Gh is the mass flux of the hot stream:

$$Gh = \frac{4 \widehat{mh}_b\, Np}{Ntt\, \pi\, Dti^2} \tag{32}$$

The variation of the heat transfer coefficients presented above with temperature is considered through the evaluation of their values using physical properties evaluated at each point of the discretization grid. Further accuracy can be attained using correction factors that consider the values of the physical properties at the tube wall temperature.

3.3.2. Air stream

The airstream heat transfer coefficient is based on the following correlation (Serth, 2007):

$$Nuc_{p,r,j} = 0.38 Rec_{p,r,j}^{0.6} Prc_{p,r,j}^{1/3} \left(\frac{Aot}{Ar} \right)^{-0.15} \tag{33}$$

where Ar is the total external surface area of the root tube per unit length.

The corresponding expressions of the Nusselt and Reynolds numbers are:

$$Nuc_{p,r,j} = \frac{hc_{p,r,j} Dte}{kc_{p,r,j}} \tag{34}$$

$$Rec_{p,r,j} = \frac{Dte\, Gc}{\mu c_{p,r,j}} \tag{35}$$

where $kc_{p,r,j}$ and $\mu c_{p,r,j}$ are the thermal conductivity and viscosity of the air stream, $hc_{p,r,j}$ is the heat transfer coefficient of the airflow, Dte is the outer tube diameter, and Gc is the air mass flux.

The air mass flux is given by:

$$Gc = \frac{mc_{tot}}{Aface\, FAR} \tag{36}$$

where $Aface$ is the projected area considering the entire bank and FAR is the minimum free area ratio. The expressions for the evaluation of $Aface$ and FAR are:

$$Aface = Nbay\, Nbbay\, W\, L \tag{37}$$

$$FAR = 1 - \frac{Dte + 2Nf\, Lf\, tf}{Ltp} \tag{38}$$

where W is the bundle width, Nf is the number of fins per unit length, Lf is the fin height, tf is the fin thickness, and Ltp is the tube pitch.

The heat transfer area per unit length of the finned tubes is given by:

$$Aot = Ab + Aof \tag{39}$$

where Ab is the exposed area of the root tube and Aof is the fin area:

$$Ab = \pi\, Dte (1 - tf\, Nf) \tag{40}$$

$$Aof = 2Nf \frac{\pi}{4} \left(Df^2 - Dte^2 \right) + \pi\, Df\, tf\, Nf \tag{41}$$

where Df is the fin diameter ($Df = Dte + 2Lf$).

3.3.3. Overall heat transfer coefficient

The expression of the overall heat transfer coefficient is:

$$U_{p,r,j} = \frac{1}{\left(\frac{1}{hh_{p,r,j}} + \widehat{Rfh} \right) \left(\frac{Aot}{\pi\, Dti} \right) + \frac{Aot \ln\left(\frac{Dte}{Dti} \right)}{2\pi\, \widehat{kt}} + \frac{1}{\eta t_{p,r,j} hc_{p,r,j}} + \frac{\widehat{Rfc}}{\eta t_{p,r,j}}} \tag{42}$$

where $\widehat{Rfh}$ and $\widehat{Rfc}$ are the fouling factors for the hot and air streams, respectively, and ηt is the finned surface's overall efficiency, which is related to the fin efficiency, ηf, according to the following expression:

$$\eta t_{p,r,j} = \left(\frac{Aot - Aof}{Aot} \right) + \eta f_{p,r,j} \left(\frac{Aof}{Aot} \right) \tag{43}$$

where ηf can be calculated by:

$$\eta f_{p,r,j} = \frac{\tanh\left(mf_{p,r,j}\, Lfe \right)}{mf_{p,r,j}\, Lfe} \tag{44}$$

$$mf_{p,r,j} = \sqrt{\left(\frac{2h'_{p,r,j}}{\widehat{kf}\, tf} \right)} \tag{45}$$

$$Lfe = Lf \left(1 + \frac{tf}{2Lf} \right) \left[1 + 0.35 \ln\left(\frac{Df}{Dte} \right) \right] \tag{46}$$

$$h'_{p,r,j} = \frac{hc_{p,r,j}}{1 + \widehat{Rfc}\, hc_{p,r,j}} \tag{47}$$

4. Fluid dynamic model

4.1. Hot stream

The hot stream pressure gradient due to the friction loss inside the tubes can be calculated locally using the model discretization. However, the variation of the physical properties implies the existence of different

flow resistances for each tube row in the same pass, which implies a nonuniformity of the flow rates among these tube rows. Alternatively, the proposed model employs a simplification based on the assumption of a uniform distribution of the flow rate among different tube rows of the same pass. The pressure drop of the hot stream in the tube rows of the same pass is evaluated by the average pressure drop in these tube rows.

The pressure drop along the tube length of a row can be calculated by:

$$\Delta Phf_{p,r} = \sum_{j=1}^{J} \frac{fh_{p,r,j}\, Gh^2 (L/J)}{2\, \rho h_{p,r,j}\, Dti}\ ,\ \forall p;\ \forall r \tag{48}$$

where Gh is the mass flux.

Therefore, the average pressure drop of each pass is given by:

$$\Delta Phfr_p = \frac{\sum_{r=1}^{R} \Delta Phf_{p,r}}{R},\ \forall p \tag{49}$$

Finally, the total pressure drop due to friction loss along the tubes is calculated by:

$$\Delta Phft = \sum_{p=1}^{Np} \Delta Phfr_p \tag{50}$$

The friction factor evaluation depends on the Reynolds number range. For $Reh \geq 10000$, the friction factor is obtained by the following equation (Serth, 2007):

$$fh_{p,r,j} = 0.4137 \left(Reh_{p,r,j}\right)^{-0.2585} \tag{51}$$

For $Reh < 2300$, the theoretical analysis yields:

$$fh_{p,r,j} = \frac{64}{Reh_{p,r,j}} \tag{52}$$

For Reynolds numbers between 2300 and 10000, the same interpolation procedure employed in Eq. (28) is also used to determine the friction factor.

The pressure drops in the header inlet and outlet, for turbulent and laminar regimes, are given by (Serth, 2007):

$$\Delta Phrin = \begin{cases} \dfrac{0.25 Gh^2}{2\, \rho hin}, & Rehin \geq 2300 \\ \dfrac{Gh^2}{2\, \rho hin}, & Rehin < 2300 \end{cases} \tag{53}$$

$$\Delta Phrout = \begin{cases} \dfrac{0.25 Gh^2}{2\, \rho hout}, & Rehout \geq 2300 \\ \dfrac{0.75 Gh^2}{2\, \rho hout}, & Rehout < 2300 \end{cases} \tag{54}$$

where $Rehin$ and ρhin are the Reynolds number and density of the hot stream at the heat exchanger inlet and $Rehout$ and $\rho hout$ are the corresponding value at the heat exchanger outlet. When there are more than one pass ($Np > 1$), the fluid flow changes its direction in a 180° turn in the header (the number of 180° turns is equal to the number of passes minus one). The corresponding values of the pressure drops are (Serth, 2007):

$$\Delta Phrx_p = \frac{Gh^2 (1.5 + \alpha_p)}{2\, \rho h_p}\ ,\ 1 \leq p \leq Np - 1 \tag{55}$$

$$\alpha_p = \begin{cases} 0.5, & 1 \leq p \leq Np-1 \quad \text{and} \quad Rehx_p \geq 2300 \\ 1.75, & 1 \leq p \leq Np-1 \quad \text{and} \quad Rehx_p < 2300 \end{cases} \tag{56}$$

where $Rehx_p$ and ρh_p are the Reynolds number and density of the hot stream at the heat exchanger header at the outlet of pass p.

The pressure drop on the nozzles is calculated depending on the flow regime:

$$\Delta Pn = \begin{cases} 7.5{\cdot}10^{-4} \dfrac{Gn^2}{s}, & \overline{Rehn} > 2300 \\ 1.5{\cdot}10^{-3} \dfrac{Gn^2}{s}, & \overline{Rehn} < 2300 \end{cases} \tag{57}$$

$$\overline{Rehn} = \frac{Gn\ Dti}{\overline{\mu h}} \tag{58}$$

$$\overline{\mu h} = \frac{\overline{\mu h}_{in} + \overline{\mu h}_{out}}{2} \tag{59}$$

where Gn is the mass flux at the nozzle, s is the average specific gravity of the hot stream, $\overline{Rehn}$ is the Reynolds number at the flow in the nozzle, and An is the flow area per nozzle.

Finally, the total tube-side pressure drop is the sum of the pressure drops in all of the elements described above:

$$\Delta Ph = \sum_{p=1}^{Np-1} \Delta Phrx_p + \Delta Phrin + \Delta Phrout + \Delta Phft + \Delta Pn \tag{60}$$

4.2. Air stream

The majority of the models presented in the literature consider a fixed air flow rate. However, it is well known that the pressure drop across the tube bundle for a given flow rate must match the head of the fan for that flow rate, as pointed out by Carvalho et al. (2019). Thus, the airflow rate is not an a priori fixed value, but a consequence of the mechanical energy balance for the combined tube bundle and fan, which needs to be solved simultaneously.

The mechanical energy balance of the fan-tube bundle system is given by:

$$\widehat{\rho} c_{in} \left(\frac{vc_{in}^2}{2} + \frac{\widehat{P}in}{\widehat{\rho} c_{in}} + \widehat{z}_{in} \widehat{g} \right) = \rho c_{out} \left(\frac{vc_{out}^2}{2} + \frac{\widehat{P}out}{\rho c_{out}} + \widehat{z}_{out} \widehat{g} \right) - \dot{w}fan + \Delta Pc \tag{61}$$

where the subscripts in and out represent the air flow entering and leaving the set tube bundle + fan, ΔPc is the pressure drop of the airflow across the tube bundle and associated parts (e.g. plenum, grids, etc.), P is the pressure, vc is the airflow velocity, z is the elevation, $\dot{w}fan$ is the pressure variation predicted by the fan curve and $\widehat{g}$ is the gravity acceleration.

Regardless of whether the air cooler draft is forced or induced, the inlet air velocity is assumed to be equal to zero. Additionally, neglecting the gravitational potential energy changes, and recognizing that $\widehat{P}out = \widehat{P}in$ one gets:

$$\dot{w}_{fan} = \rho c_{out} \frac{vc_{out}^2}{2} + \Delta Pc \tag{62}$$

Therefore, the airflow rate corresponds to the solution of the nonlinear equation depicted in Eq. (62).

The outlet air velocity depends on the air cooler type, as follows:

$$vc_{out}^{induced} = \frac{q_{out}}{Nbay\ Nfanbay \left(\frac{\pi}{4}\ Dfan^2 \right)} \tag{63}$$

$$vc_{out}^{forced} = \frac{q_{out}}{Aface} \tag{64}$$

$$q_{out} = mc_{tot} / \rho c_{out} \tag{65}$$

where q_{out} is the volumetric flow rate of the air stream that leaves the air cooler, associated with a density value equal to the average air density of the last row of the last pass:

$$\rho c_{out} = \frac{\sum_{j=1}^{J} \rho c_{1,1\,j}}{J} \tag{66}$$

4.2.1. Fan curve

The fan curve can be represented, without loss of generality, by a third-degree polynomial:

$$\dot{w}_{fan} = \widehat{AP}_{fan} + \widehat{BP}_{fan} q_{fan} + \widehat{CP}_{fan} q_{fan}^2 + \widehat{DP}_{fan} q_{fan}^3 \tag{67}$$

where q_{fan} is the air volumetric flow rate in each fan, given by:

$$q_{fan} = \frac{mc / \rho c_{fan}}{Nbay\ Nfanbay} \tag{68}$$

The position of the fan depends on the air cooler draft type. The fan is located above the tube bundle in the induced draft and is located below the tube bundle in the forced draft. Therefore, ρc_{fan} in Eq. (68) corresponds $\widehat{\rho} c_{in}$ for the forced draft alternative and ρc_{out} for the induced draft alternative.

4.2.2. Tube bundle pressure drop

The air stream pressure drop through the tube bundle, ΔPc, is given by (Serth, 2007):

$$\Delta Pc = 1.1 \frac{2fc\ Gc^2\ Nr}{\overline{\rho c}_{tot}} \tag{69}$$

where fc is the air-side friction factor and $\overline{\rho c}_{tot}$ is the average of the density in the tube bundle:

$$\overline{\rho c}_{tot} = \frac{\sum_{p=1}^{Np} \sum_{r=1}^{R} \sum_{j=1}^{J} \rho c_{p,r,j}}{J\ R\ Np} \tag{70}$$

The air-side friction factor expression is:

$$fc = \left(1 + \frac{2e^{-a/4}}{1+a}\right)\left(0.021 + \frac{27.2}{Reeff} + \frac{0.29}{Reeff^{0.2}}\right) \tag{71}$$

where a and $Reeff$ are calculated by:

$$a = \frac{Ltp - Df}{Dte} \tag{72}$$

$$Reeff = \overline{Rec}\ \frac{sf}{Lf} \tag{73}$$

where sf is the fin spacing and $\overline{Rec}$ is given by:

$$\overline{Rec} = \frac{\sum_{p=1}^{Np} \sum_{r=1}^{R} \sum_{j=1}^{J} Rec_{p,r,j}}{J\ R\ Np} \tag{74}$$

4.2.3. Energy consumption

The corresponding energy consumption that determines the operational cost is given by (Serth, 2007):

$$Wused = \frac{BHP}{\widehat{\eta sr}\ \widehat{\eta motor}} \tag{75}$$

where $\widehat{\eta sr}$ and $\widehat{\eta motor}$ are the efficiencies in the speed reducer and the motor, respectively, and BHP is the brake horsepower.

The brake horsepower can be evaluated by:

$$BHP = \frac{\dot{w}_{fan}\ qfan}{\widehat{\eta fan}} \tag{76}$$

where $\widehat{\eta fan}$ is the fan efficiency. Alternatively, BHP can be evaluated by the corresponding fan curve, if available.

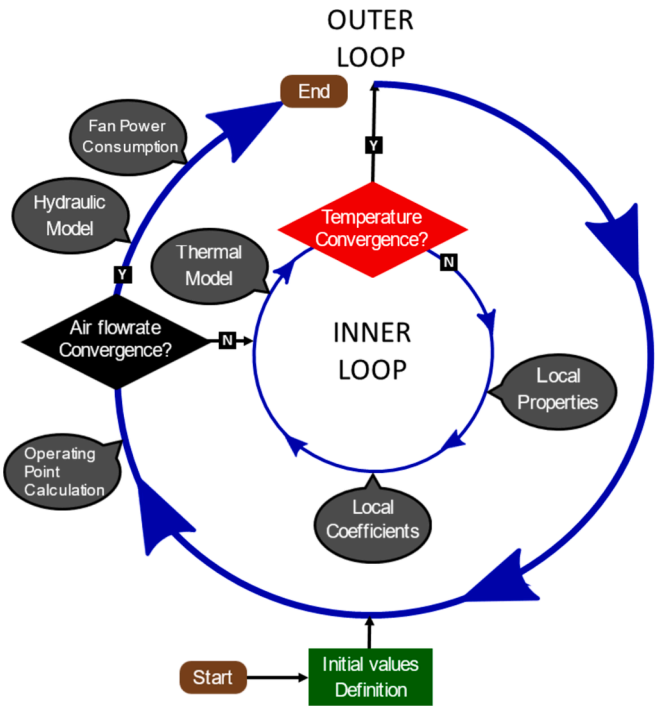

Fig. 5. Flowchart for the iterative procedure method.

5. Simulation

The air cooler mathematical model is solved in an iterative scheme composed of two convergence loops, as illustrated by Fig. 5.

The inner loop corresponds to the thermal model, encompassing the discretized equations of the energy balances, including the correlations for the evaluation of the heat transfer coefficients. The airflow rate in this loop corresponds to the value obtained in the outer loop. For an initial set of values of temperatures, the physical properties and heat transfer coefficients can be evaluated. Then, updated values of the temperature field can be determined through the solution of the linear system of the discretized energy balances. The process is then repeated until convergence of the temperatures.

The outer loop corresponds to the solution of the fluid dynamic model, which corresponds to the determination of the airflow rate through the solution of the mechanical energy balance equation. The physical properties depend on the temperature and are evaluated according to the temperature field determined in the inner loop.

The complete process converges when the modification of the airflow rate between two consecutive iterations is smaller than a given tolerance.

6. Optimization

6.1. Problem formulation

The objective function of the optimal design problem corresponds to the minimization of the total annualized costs (TAC), including capital ($Cinv$), maintenance ($Cmai$), and operating costs (Cop):

$$TAC = \widehat{CRF}\ Cinv + Cmai + Cop \tag{77}$$

The evaluation of each term of Eq. (77) is based on Conradie et al. (1998).

The constraints of the design problem involve geometric constraints, tube velocity bounds, hot stream pressure drop upper bound, and hot stream maximum outlet temperature.

The geometric constraints represent relations between the air cooler

dimensions that must be obeyed in a feasible design, as follows.

A minimum gap between adjacent fin tips is required:

$$Ltp \geq Df + \widehat{at} \tag{78}$$

The fan must fit inside the bundle:

$$NbbayW \geq Dfan + 2\widehat{fd} \tag{79}$$

$$Dfan - 2fl \leq L - Lfanp(Nfanbay - 1) \tag{80}$$

Finally, the area of the fans must be at least 40 % of the bay face area:

$$\frac{\pi}{4} Nfanbay\ Dfan^2 \geq 0.4 Nbbay\ W\ L \tag{81}$$

To avoid erosion and vibration, a maximum velocity for the hot stream is imposed. To avoid fouling, a minimum velocity is defined. The hot stream velocity varies along the tube, because of changes in density. Nonetheless, the maximum velocity is reached in the inlet, vh_{IN} (hotter end associated with the highest density value), and the minimum velocity is reached in the outlet, vh_{OUT} (colder end associated with the smallest density value). Therefore, the corresponding constraints are:

$$vh_{IN} \geq \widehat{vhmax} \tag{82}$$

$$vh_{OUT} \leq \widehat{vhmin} \tag{83}$$

where $\widehat{vhmax}$ and $\widehat{vhmin}$ are the corresponding upper and lower bounds on the hot stream flow velocities.

A maximum pressure drop is also established for the hot stream flow:

$$\Delta Ph \leq \Delta\widehat{Phmax} \tag{84}$$

The thermal task to be executed is represented by the specification of a maximum outlet temperature of the hot stream:

$$Th_{out} \leq \widehat{Thmax} \tag{85}$$

6.2. Optimization method

Several approaches can be used to solve the above problem: Metaheuristics, Mathematical Programming, and the recently developed Set Trimming followed by Smart Enumeration (Costa and Bagajewicz, 2019). For the goal of attaining a globally optimal design, Metaheuristics is not a choice because, by construction, these methods cannot guarantee global optimality. In turn, Mathematical Programming needs global optimization solvers to be used (i.e. Baron, Antigone, and a few others). Indeed, one could build the nonconvex DAE optimization model, reformulate it as a mixed integer nonlinear optimization model (MINLOM), and try to solve it. This alternative was not explored, especially because when confronting similar complex and highly nonconvex models (Kim et al., 2023; Souza et al., 2023), serious convergence difficulties were experienced, to the point that sometimes the global solvers failed to obtain the global optimum or no feasible solution was attained. To avoid these risks, and because it has proven to be faster in our experience, Partial Set Trimming followed by Smart Enumeration (Costa and Bagajewicz, 2019) was employed. According to this optimization approach, the search space is composed of all design candidates. Each candidate is represented by a combination of the values of the discrete design variables, composed of number of bays, number of tube bundles per bay, number of fans per bay, number of tubes per row, number of tube passes and tube rows, tube pitch ratio, tube length, finned tube option (which is represented by a combination of tube diameter, fin height, number of fins per unite length, and fin thickness), and fan option (including the fan diameter and fan curve).

6.2.1. Set Trimming

The Set Trimming step corresponds to the sequential application of the inequality constraints of the problem. The candidates that are not feasible in a given constraint are eliminated from the search. Therefore, there is a gradual reduction in the number of candidates along the search, which contributes to the computational efficiency of the method. An important aspect of Set Trimming is the utilization of special computational routines for handling large sets of data, instead of using slow loops based on the evaluation of a single candidate at a time.

The sequence of the application of the constraints in the Set Trimming step corresponds to the order of the presentation of the constraints as depicted above. Aiming at reducing the computational effort, this sequence is based on a crescent order of the complexity of each constraint, i.e. the more complex constraints are evaluated later, when a smaller number of candidates has left.

However, because of its nature, the pressure drop and outlet temperature constraints (Eq. (84) and Eq. (85)) demand the solution of the entire mathematical model, which hinders their utilization in the Set Trimming step. This obstacle is overcome by the substitution of these constraints in the Set Trimming by proxies.

The Proxy Set Trimming is the substitution of the constraint by a simpler relation that is a limit of the original constraint. Therefore, part of candidates that are not feasible according to a given constraint is eliminated, without the need to solve the entire mathematical model.

The Proxy Set Trimming of the maximum pressure drop of the hot stream corresponds to the substitution of the original constraint in Eq. (84) by:

$$\Delta P_{LB} \leq \Delta\widehat{Phmax} \tag{86}$$

where ΔP_{LB} is a lower bound of the hot stream pressure drop.

The pressure drop lower bound is built through the application of Eq. (60) with uniform values of the physical properties and friction factor. These values are selected to provide the corresponding lower bound on the pressure drop. The friction factor in Eqs. (51) and (52) is assumed equal to its corresponding value at the heat exchanger inlet, which is the smallest value along the entire heat exchanger. The hot stream density in Eqs. (48), (53), (54), and (55) is associated with a maximum value. Therefore, the resultant evaluated pressure drop is a lower bound of the actual pressure drop.

The Proxy Set Trimming of the maximum outlet hot stream temperature (Eq. (85)) is associated with a lower bound on the required area of the heat exchanger. If the actual outlet temperature of the hot stream is lower than the required outlet temperature, then it means that the heat exchanger area is higher than the required area, i.e. the constraint in Eq. (85) is equivalent to:

$$A \leq A_{req} \tag{87}$$

Because the evaluation of A_{req} demands the solution of the entire mathematical model, the corresponding Proxy Set Trimming uses a lower bound based on the analytical solution through the LMTD method:

$$A \leq A_{LB} \tag{88}$$

where:

$$A_{LB} = \frac{\widehat{Q}}{U_{UB}\Delta T_{UB}} \tag{89}$$

where $\widehat{Q}$ is the design heat load, ΔT_{UB} is an upper bound on the average temperature difference along the heat transfer surface and U_{UB} is an upper bound on the overall heat transfer coefficient.

Here, U_{UB} is calculated considering all the values of physical properties that lead to the highest possible value of the overall heat transfer coefficient, namely, the largest Reynolds number obtained using the largest velocity, the largest density, and the lowest viscosity in the tubes within the expected temperature range. The same scheme is applied to the evaluation of the Prandtl number and for the efficiency of the finned surface.

According to the LMTD method, the logarithmic mean temperature

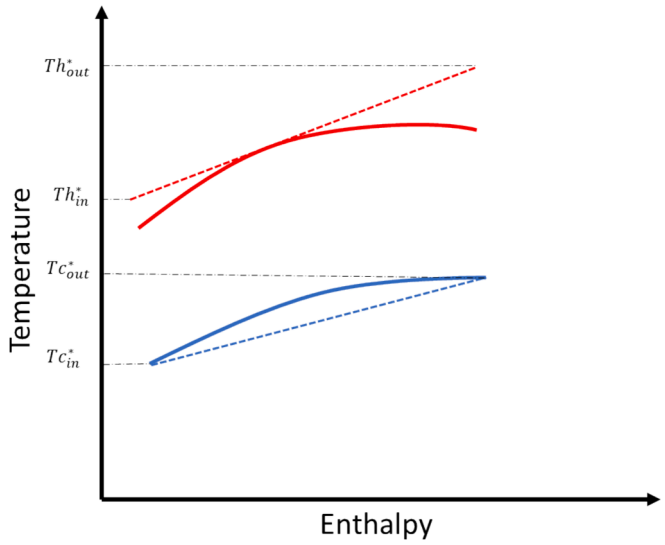

Fig. 6. Temperature vs. enthalpy diagram (dashed lines: upper and lower bounds of the temperature difference).

difference is the highest mean temperature difference for any heat exchanger configuration. However, this fact is based on the assumption of uniform heat capacity that provides the analytical solution associated with the LMTD method. Therefore, the expression for evaluation of ΔT_{UB} corresponds to the evaluation of the logarithmic mean temperature difference assuming uniform heat capacities that are tangent and secant lines in a Temperature x Enthalpy diagram, as illustrated by Fig. 6.

Therefore, from Fig. 6, it yields:

$$\Delta T_{UB} = \frac{\left(Th^*_{in} - Tc^*_{out}\right) - \left(Th^*_{out} - Tc^*_{in}\right)}{\ln\left[\frac{\left(Th^*_{in} - Tc^*_{out}\right)}{\left(Th^*_{out} - Tc^*_{in}\right)}\right]} \quad (90)$$

While any point can be chosen to draw the tangent for the hot stream, the midpoint of the curve is adopted, which is expected to be near the best point possible, the one that renders the smallest difference.

6.2.2. Smart enumeration

After the Set Trimming step, the list of the remaining candidates is considerably reduced compared with the initial search space. However, because proxies were employed during the Set Trimming (i.e. Partial Set Trimming is used), the remaining set of candidates contains some infeasible candidates together with all feasible candidates.

To avoid the simulation of all of the remaining candidates to determine if they are feasible or not, a Smart Enumeration methodology is employed, first formalized by Costa and Bagajewicz (2019) and applied to a simpler version of this problem by Carvalho et al. (2019).

First, the candidates are sorted according to a crescent order of an objective function lower bound of each candidate. This lower bound is built through the *TAC* evaluation using a lower bound of the air cooler operating costs, evaluated by a lower bound of the air pressure drop and a lower bound of the airflow rate. This pressure drop lower bound is determined, without solving the mathematical model of each candidate, using the air physical properties at the heat exchanger inlet, where, because the air is cooler, the density is higher and the viscosity is lower.

Based on this ordered candidate list, the mathematical model of each candidate is solved, starting from the candidate with the lowest value of the *TAC* lower bound. If a given candidate is infeasible, it is discarded and the search goes to the next one in the list. If the candidate is feasible, its objective function is evaluated and compared with the lowest value of the objective function calculated so far (i.e. the incumbent candidate). If the objective function is higher than the incumbent one, the candidate is discarded, otherwise, this candidate is the new incumbent. After this analysis, the search goes to the next candidate. When the lower bound of the objective function of a candidate is higher than the objective function of the incumbent, the search stops, because all of the remaining candidates have objective function values higher than the incumbent (the candidates list is in a crescent order of their objective function lower bound). This strategy always attains the global optimal solution.

Table 1
Validation: Comparison of results with an analytical solution.

Result	Serth (2007)	Proposed model
Reh	69,594	69,594
Rec	8115	8164
U (W/(m^2 K))	25.3	25.3
ΔPh (Pa)	105,490	105,643
ΔPc (Pa)	89.67	90.65
Tho (°C)	63.20	63.32
Tco (°C)	66.91	66.94

Table 2
Validation: Comparison of results with different software packages.

Result	HEXTRAN	HTRI XACE	Aspen ACOL	Aspen EDR	Discretized model
Reh	69,596	69,623	69,622	69,622	69,594
Rec	8080	8381	8155	8621	8164
hh (W/(m^2 K))	2385	2782	2805	2799	2385
hc (W/(m^2 K))	40.9	55.1	52.3	52.8	52.0
U (W/(m^2 K))	23.0	26.5	25.9	26.1	25.3
ΔPh (Pa)	108,248	112,384	107,558	107,558	105,643
ΔPc (Pa)	99.64	79.71	104.62	94.65	90.66
Tho (°C)	65.65	61.96	62.57	60.78	63.30
Tco (°C)	65.56	67.59	67.25	68.33	66.95

7. Results

7.1. Model validation

The first step in the validation involved the comparison of the results obtained using the proposed model with constant physical properties with an analytic solution. In this case, a case study proposed by Serth (2007), where a liquid hydrocarbon is cooled is used. The simulation output using the developed code was compared with the results presented in Serth (2007), as shown in Table 1. The simulation results of the developed code match very closely with the results from Serth (2007), which indicates that the numerical simulation converges to the analytical solution when the assumptions of constant physical properties are valid.

A second validation step involved the comparison of the proposed model with solutions obtained using commercial software. The analysis addressed the same air cooler described in Serth (2007) with fixed values of the hydrocarbon properties, but the air properties were evaluated using the internal correlations of each software considering their variation with the temperature. The results using the proposed model employed the air properties correlations described in Souza et al. (2018).

Table 2 shows the results reported by Serth (2007) that were obtained using the commercial computer codes HEXTRAN, HTRI XACE, and Aspen ACOL. Additionally, Table 2 also contains the results obtained in the current paper using the software Aspen EDR v10.

The set of results in Table 2 indicates a slight dispersion of the outputs related to different software programs. The results of outlet temperatures were always within the minimum and maximum values predicted by the different software.

Table 3
Example: Data of the streams.

Stream data	Tube-side	Airside
Mass flow rate (kg/s)	50	200
Inlet temperature (°C)	130	15
Fouling factor (m^2K/W)	0.00017611	0

Table 4
Example: Data of the simulated air cooler.

Design data	Value
Area (m^2)	4150
Number of tubes per row	38
Number of tube passes	4
Number of rows	4
Outer diameter (m)	0.0254
Tube pitch (m)	0.0508
Tube length (m)	15
Fin length (m)	0.009525
Number of fins (m^{-1})	393
Fin thickness (m)	0.000381
Number of bays	1
Number of fans per bay	3
Fan diameter (m)	3.2
Number of bundles per bay	2

7.2. Simulation results

The utilization of a simulation approach based on the numerical resolution of the conservation equations is particularly important when there are large variations in the physical properties. To illustrate the importance of this issue, a simulation result is presented here considering an air cooler with a hot stream composed of engine oil, a viscous fluid with properties that vary significantly with temperature. The data of the streams are depicted in Table 3 and the geometry of the simulated heat exchanger is present in Table 4. The physical properties of this fluid were obtained from the data reported by Bergman et al. (2017).

The corresponding profiles of the temperatures along the different passes are shown in Fig. 7a and b. Fig. 7a shows a continuous reduction of the temperature of the hot stream throughout the different passes. The airstream flows from bottom to top, therefore the temperature increases from the last pass (Pass 4) towards the first pass (Pass 1), as shown in Fig. 7b. The modifications of the air temperature profile along the tube length in the different passes, depicted in Fig. 7b, is associated with the larger increase of the air temperature near the entrance of each pass due to the higher temperature of the hot stream at this region and the higher value of the hot stream convective coefficient associated with the entry region.

Fig. 8a shows the profiles of the Reynolds number for the different passes. It is interesting to observe that the Reynolds number varies significantly, causing the flow regime to change, which illustrates the large variation of the physical properties in this problem. The reduction of the temperature of the hot stream along the flow is associated with an increase in the oil viscosity, which brings a reduction in the Reynolds number (that contributes to the large pressure drop in this heat exchanger). Consequently, there are three different regimes along with the tube-side flow. The average Nusselt number in each pass is shown in Fig. 8b, where it is possible to observe a decrease along with the different passes due to the reduction of the Reynolds number.

7.3. Comparisons with the LMTD method: Implications for the design

As shown in the Introduction, a significant number of papers addressed the utilization of optimization techniques for the solution of the air cooler design problem using the LMTD and ε-NTU methods, which are analytical solutions based on the assumption of uniform physical properties.

Therefore, it is important to analyze the implication of the utilization of these methods for the design of air coolers when compared with the proposed discretized model. This analysis was conducted by applying the LMTD method and the discretized model for the simulation of the air cooler described above. Both approaches employed equivalent equations for the evaluation of the heat transfer coefficients (because of the lumped nature of the coefficients in the LMTD method, the average convective heat transfer coefficient of the tube-side in the LMTD method was evaluated using the integration of Eqs. (27–32)). Additionally, the physical properties employed for the evaluation of the heat transfer

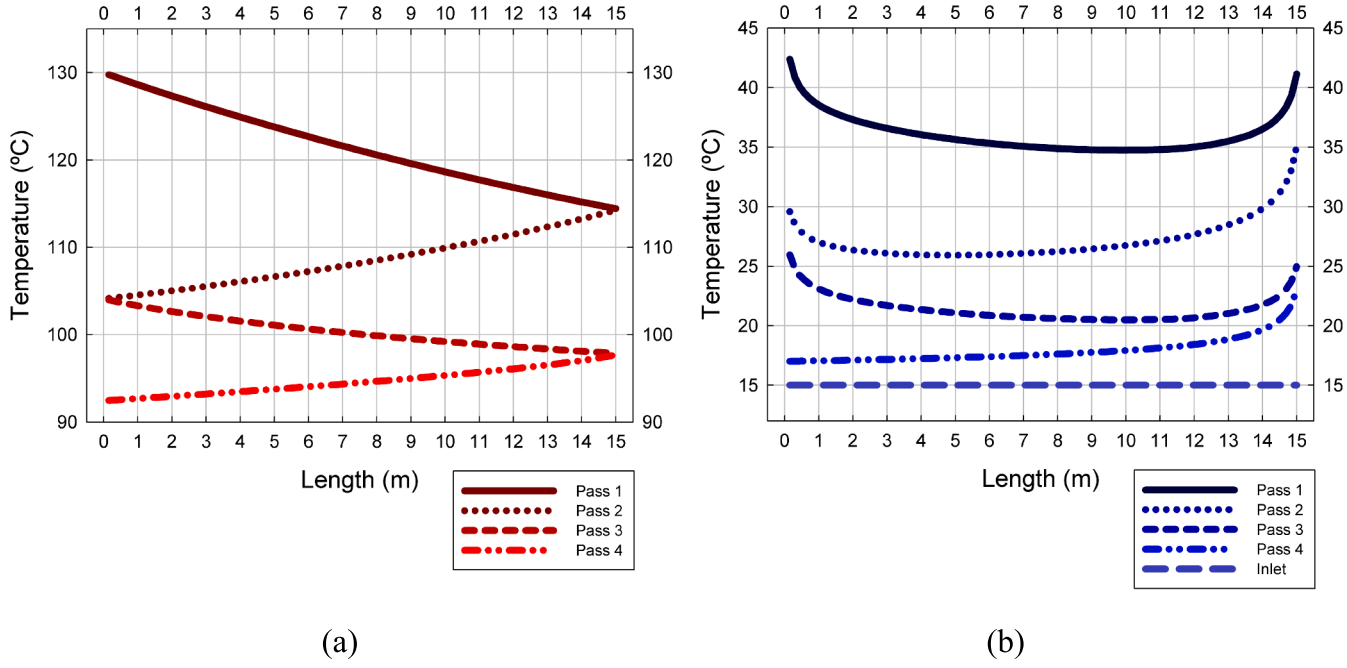

Fig. 7. Temperature profiles: (a) tube-side, (b) air-side.

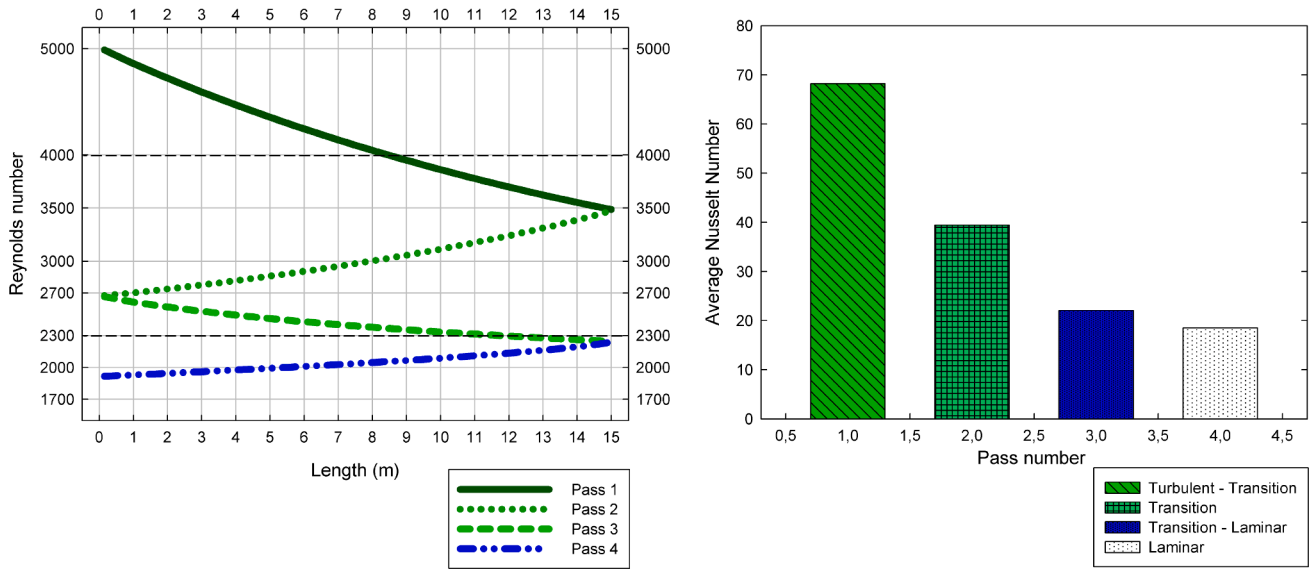

(a) (b)

Fig. 8. (a) Tube-side Reynolds number profile, (b) Tube-side average Nusselt number in each pass.

Table 5
Comparison with LMTD of the proposed example.

	Discretized Model	LMTD method
Oil outlet temperature (°C)	92.47	88.15
Air outlet temperature (°C)	36.07	38.39

coefficients in the LMTD method were based on average temperatures. Thus, the application of the LMTD method involved an outer loop to promote convergence of the value of the average temperature based on the actual outlet temperature. The equations for the evaluation of the correction factor of the LMTD were based on Souza et al. (2018).

The results of this comparison are shown in Table 5, where it is possible to observe that the LMTD method predictions are too optimistic compared to the discretized model. The calculated oil temperature reduction from the air cooler inlet to the outlet is 12 % higher for the LMTD method than the corresponding value calculated using the discretized model.

This behavior can be explained by the profiles present in Fig. 9, which compare the values of the convective heat transfer coefficient along the passes evaluated using the discretized model with the uniform value adopted by the LMTD method. It can be observed that the uniform value adopted by the LMTD method overestimates the corresponding values evaluated by the rigorous simulation in a major part of the heat exchanger.

These differences in the model predictions can impact the design of an air cooler. The optimistic result of the LMTD method compared to the more accurate discretized model implies that “false positives” can take place, i.e. the air cooler is found viable for a given thermal task using the LMTD method, but it is not viable according to a more accurate model.

To investigate this deviation, a simulation of a large list of air coolers was performed using the proposed discretized model and the LMTD method applied to the stream data depicted in Table 3. The results were compared considering two design scenarios: a target outlet temperature of the oil stream lower than 80 °C and lower than 90 °C. The list of investigated air coolers is based on a sample of the search space employed by Souza et al. (2018) in a design optimization problem. The

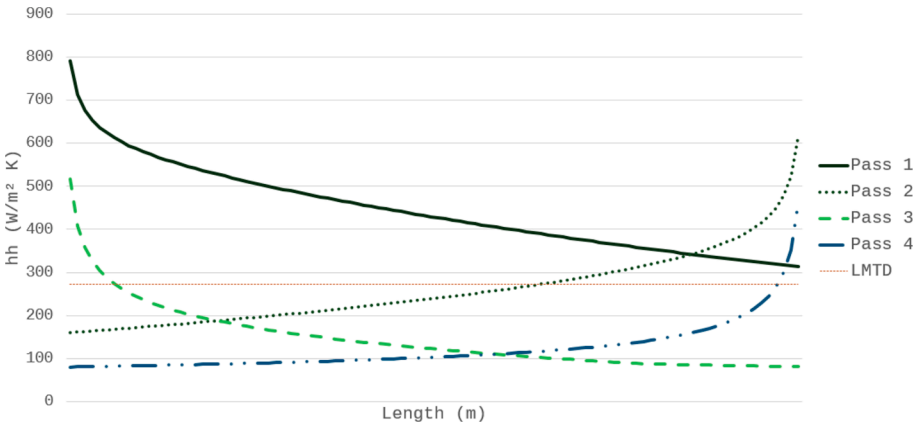

Fig. 9. Hot stream convective heat transfer coefficient profiles.

Table 6
Standard values of the design variables.

Variable	Values
Number of bays	1, 2
Number of bundles per bay	1, 2, 3
Number of fans per bay	1, 2
Number of tubes per row	35, 38, 41, 44, 47, 50, 53, 56
Pitch Ratio	2, 2.5
Fan Diameter	1.2, 2.2, 3.2, 4.2, 5.2
Tube length	4.572, 6.096, 7.315, 9.114, 10.973

Table 7
Standard values of the air cooler configurations.

Number of tube passes	Number of rows
1	3
1	4
1	5
1	6
3	3
4	4
5	5
6	6
2	4

Table 8
Standard values of the finned tubes.

Outer diameter (m)	Fin height (m)	Number of fins (m^{-1})	Fin thickness (m)
0.0254	0.00635	275	0.000381
0.0254	0.00635	393	0.000381
0.0254	0.009525	275	0.000381
0.0254	0.009525	393	0.000381
0.0254	0.015875	393	0.000330

investigated list contains 5,256 different air coolers.

According to the LMTD method, there are 16 heat exchangers in the sample able to fulfill the design task to cool the oil stream from the inlet temperature to a temperature value lower than 80 °C. However, the simulation of these heat exchangers using the discretized model indicated that none of them are feasible, i.e. they are all "false positives". Repeating the analysis for a less stringent design task, that is, an outlet temperature target of 90 °C, it is possible to identify 331 heat exchangers that can fulfill the design task according to the LMTD method. However, equivalent results using the discretized model indicated that 128 of those alternatives are not feasible, i.e. about 39 % of the design solutions confirmed by the LMTD method are "false positives".

As it is illustrated in Fig. 9, the main reason for the existence of "false positives" in this example related to LMTD-like approaches is that these approaches use the average temperatures to calculate physical properties in the model. Discrepancies between the real values of these properties as a function of the temperatures inside the air cooler can be high, like in the case of viscous fluids. If that happens, the heat transfer coefficient changes inside the exchanger may not be appropriately described by an uniform value based on an average temperature.

7.4. Optimization results

A design example is solved here using the proposed optimization approach. The equipment is an induced draft air cooler. The discrete values of the design variables employed in the optimization problem are given by typical manufacture values (Serth, 2007; Souza et al., 2018; Chart Industries, 2024), according to Tables 6, 7, 8, and 9. The hot stream nozzles correspond to a 5 in diameter Sch 40.

The design problem was solved using Partial Set Trimming followed by Smart Enumeration. The algorithm was implemented in the GAMS language, using a custom code specifically developed to solve the problem. A traditional solver was not employed directly for the optimization. However, during the enumeration phase of the algorithm, the CPLEX solver was used recurrently with a dummy objective function. This allowed CPLEX to solve the underlying system of linear equations. The use of CPLEX in this context was necessary to ensure accurate resolution of the linear systems, although it was not utilized for the primary objective function.

The hot stream is an engine oil with a flow rate of 20 kg/s that must be cooled from 147 °C to 120 °C. The fouling factors of the oil and the air are 0.00017611 m^2°C/W and 0 m^2°C/W. The maximum hot stream pressure drop is 80895 Pa and the hot stream velocity must be between 1 m/s and 2.5 m/s.

The design of the optimal air cooler is depicted in Table 10. The optimal values of the pressure drop and hot stream outlet temperature are shown in Table 11. The values of the heat transfer coefficients are shown in Table 12.

Table 13 shows the number of candidates at the start of the search and after the application of each constraint during the Set Trimming step. It can be observed that the number of solution candidates is reduced along the sequence of constraints. In the end, only 4,013 are left, which is equivalent to 1.86 % of the original search space.

The application of Smart Enumeration identifies the global optimum through the simulation of 83 candidates. Therefore, the global optimum

Table 9
Fan options.

Fan diameter (m)	A	B	C	D
1.2	889.7	−0.0207	$2.520 \cdot 10^{-7}$	$-1.755 \cdot 10^{-12}$
2.2	1505	−0.0394	$4.495 \cdot 10^{-7}$	$-2.213 \cdot 10^{-12}$
3.2	1800	−0.03969	$4.108 \cdot 10^{-7}$	$-2.008 \cdot 10^{-12}$
4.2	−1104	0.05244	$-6.579 \cdot 10^{-7}$	$2.434 \cdot 10^{-12}$
5.2	238.9	0.007608	$-8.713 \cdot 10^{-8}$	$1.397 \cdot 10^{-13}$

Table 10
Optimal air cooler: Design variables.

Variable	Optimal value
Number of bays	1
Number of bundles per bay	1
Number of fans per bay	2
Number of tubes per row	53
Number of tube passes	3
Number of rows	3
Pitch ratio	2.5
Fan diameter (m)	3.2
Tube length (m)	10.973
Tube outlet diameter (m)	0.0254
Fin height (m)	0.006
Number of fins per length (1/m)	393
Fin thickness	0.00381

Table 11
Optimal air cooler: Pressure drop and hot stream outlet temperature.

Variable	Optimal results
Hot stream pressure drop (Pa)	68,780
Airstream pressure drop (Pa)	16.42
Oil outlet temperature (°C)	119.92

Table 12
Optimal air cooler: Heat transfer coefficients.

Variable	Minimum	Average	Maximum
Overall heat transfer coefficient (W/(m^2 °C))	11.03	14.23	24.06
Oil heat transfer coefficient (W/(m^2 °C))	144.57	236.45	661.86
Air heat transfer coefficient (W/(m^2 °C))	38.39	38.58	39.17

Table 13
Number of candidates remaining after each constraint applied.

Start	Eq. (79)	Eq. (80)	Eq. (81)	Eq. (82)	Eq. (83)	Proxy of Eq. (84)	Proxy of Eq. (85)
216,000	194,400	143,640	114,174	9,306	4,280	4,146	4,013

Table 14
Computational time comparison.

	Souza et al. (2018)	This work
Computational time (s)	60	8.9

is identified through the simulation of only a small fraction of the initial search space, 0.038 %.

7.5. Computational performance

The optimization problem described above was solved in 2 min and 16 s using a Lenovo Thinkpad E14 laptop equipped with an 11th Generation Intel® Core i7-1165G7 processor (4 cores, 8 threads, base clock 2.8 GHz, turbo up to 4.7 GHz), 32 GB DDR4 RAM (3200 MHz), running Windows 11. This performance is considered reasonable for practical purposes.

To compare the computational performance of the proposed approach with previous work, the design problem described in Souza et al. (2018) was solved using the proposed approach and the mathematical programming problem presented in the original paper. To provide a direct comparison, physical properties and the air flow rate were assumed constant, according to the problem formulation of Souza et al. (2018).

Table 14 shows the corresponding computational times of each solution approach. The proposed approach found the same solution as Souza et al. (2018) in only 15 % of the computational time of the mathematical programming approach.

8. Conclusions

The solution to the optimal design problem of air coolers using a discretized mathematical model is presented in this paper. The model was validated through a comparison with commercial software programs. The proposed model is particularly important when the hot stream presents large variations of the physical properties. In such situations, it is essential to consider physical properties and heat transfer coefficients varying locally. When exploring this design problem, it is shown that the deviations associated with the traditional approaches based on uniform physical properties can accept exchangers that cannot fulfill the thermal task.

The proposed optimization method to solve the design problem always identifies the global optimum. Numerical results indicate that it is faster than a previous approach for design optimization using Mathematical Programming. Considering that previous works that addressed the optimal design of air coolers in petroleum and chemical industries were based on analytical solutions, the proposed method can provide more accurate solutions.

CRediT authorship contribution statement

Marco Thiago da C. Santos: Writing – original draft, Visualization, Validation, Software, Methodology, Investigation. **Argimiro Resende Secchi:** Writing – review & editing, Supervision, Methodology, Investigation, Conceptualization. **Miguel J. Bagajewicz:** Writing – review & editing, Supervision, Methodology, Investigation, Conceptualization. **André L.H. Costa:** Writing – review & editing, Supervision, Methodology, Investigation, Conceptualization.

Declaration of competing interest

The authors declare that they have no known competing financial interests or personal relationships that could have appeared to influence the work reported in this paper.

Acknowledgments

Marco T. C. Santos thanks the Research Support Foundation of Rio de Janeiro (FAPERJ) and Coordenação de Aperfeiçoamento de Pessoal de Nível Superior – Brasil (CAPES) for his doctorate scholarships. André L. H. Costa thanks the National Council for Scientific and Technological Development (CNPq) for the research productivity fellowship (Process 308727/2022-3) and the financial support of the Prociência Program (UERJ). Miguel Bagajewicz thanks the visiting researcher scholarship from UERJ (PAPD Program) and the support of the Federal Univerity of Rio de Janeiro (UFRJ). Argimiro R. Secchi thanks CNPq for the research productivity fellowships (Process 303587/2020-2).

Data availability

Data will be made available on request.

References

Archer, U.M., Petzold, L.R. 1998. Computer Methods for Ordinary Differential Equations and Differential-Algebraic Equations, SIAM, Ed.
Bergman, T.L., Lavine, A.S., Incropera, F.P., Dewitt, D.P., 2017. Fundamentals of Heat and Mass Transfer. Wiley.
Carvalho, C.B., Ravagnani, M.A.S.S., Bagajewicz, M.J., Costa, A.L.H., 2019. Globally optimal design of air coolers considering fan performance. Appl. Therm. Eng. 161, 114–188.
Chart Industries, The Basics of AIR-COOLED HEAT EXCHANGERS. https://www.chartindustries.com/Products/Air-Cooled-Heat-Exchangers, **2024** (accessed 28 October 2024).
Conradie, A.E., Buys, J.D., Kroger, D.G., 1998. Performance optimization of dry-cooling systems for power plants through SQP methods. Appl. Therm. Eng. 18, 25–45.
Costa, A.L.H., Bagajewicz, M.J., 2019. 110th Anniversary: On the departure from heuristics and simplified models toward globally optimal design of process equipment. Ind. Eng. Chem. Res. 58, 18684–18702.
Doodman, A.R., Fesanghary, M., Hosseini, R., 2009. A robust stochastic approach for design optimization of air cooled heat exchangers. Appl. Energy 86, 1240–1245.
Garcia, J.C.S., Giannetti, N., Varela, D.A.B., Varela, R.J., Yamaguchi, S., Saito, K., Berana, M.S., 2022. Design of a numerical simulator for finned-tube heat exchangers with arbitrary circuitry. Heat Transf. Eng. 43, 1675–1693.
Gnielinski, V., 2010. G1 Heat Transfer in Pipe Flow. VDI Heat Atlas. Springer, Berlin, Heidelberg.
González, M.T., González, G., Petracci, N.C., Urbicain, M.J., 2001. Air-cooled heat exchanger design using successive quadratic programming (SQP). Heat Transf. Eng. 22, 11–16.
Jiang, H., Aute, V., Radermacher, R., 2006. CoilDesigner: a general-purpose simulation and design tool for air-to-refrigerant heat exchangers. Int. J. Refrig. 29, 601–610.
Karami, A., Rezaei, E., Shahhosseni, M., Aghakhani, M., 2012. Optimization of heat transfer in an air cooler equipped with classic twisted tape inserts using imperialist competitive algorithm. Exp. Therm. Fluid Sci. 38, 195–200.
Kashani, A.H.A., Maddahi, A., Hajabdollahi, H., 2013. Thermal-economic optimization of an air-cooled heat exchanger unit. Appl. Therm. Eng. 54, 43–55.
Kim, S.Y., Costa, A.L.H., Bagajewicz, M.J., 2023. New robust approach for the globally optimal design of fired heaters. Chem. Eng. Res. Des. 197, 434–448.
Li, Z., Aute, V., Ling, J., 2019. Tube-fin heat exchanger circuitry optimization using integer permutation based genetic algorithm. Int. J. Refrig. 103, 135–144.
Manassaldi, J.I., Scenna, N.J., Mussati, S.F., 2014. Optimization mathematical model for the detailed design of air cooled heat exchangers. Energy 64, 734–746.
Paikert, P. 2008. Air as coolant for industrial processes: Comparison to water, In Heat Exchanger Design Handbook, Editor: G. F. Hewitt.
Ploskas, N., Laughman, C., Raghunathan, A.U., Sahinidis, N.V., 2018. Optimization of circuitry arrangements for heat exchangers using derivative-free optimization. Chem. Eng. Res. Des. 131, 16–28.
Rezaei, E., Karami, M., Alimohammad Shahhosseni, M., Aghakhani, 2012. The optimization of thermal performance of an air cooler equipped with butterfly inserts

by the use of imperialist competitive algorithm. Heat Transf. - Asian Res. 41, 214–226.
Sarfraz, O., Bach, C.K., Bradshaw, C.R., 2019. Discrete modeling of fin-and-tube heat exchangers with cross-fin conduction functionality. Int. J. Refrig. 104, 270–281.
Saunders, E.A.D., 1988. Heat Exchangers: Selection, Design and Construction. John Wiley & Sons, New York.
Serth, R.W., 2007. Process Heat Transfer: Principles and Applications, first ed. Elsevier Ltd.
Souza, A.R.C., Bagajewicz, M.J., Costa, A.L.H., 2023. Set trimming approach for the globally optimal design of sieve trays in separation columns. AIChE J. 69, e18003.
Souza, P.A., Costa, A.L.H., Bagajewicz, M.J., 2018. Globally optimal linear approach for the design of process equipment: the case of air coolers. AIChE J. 64, 886–903.